FULL PAPER

DOI: 10.1002/adem.201600607

Effects of Ag Addition on Hot Deformation Behavior of Cu–Ni–Si Alloys**

By *Huili Sun, Yi Zhang,* Alex A. Volinsky,* Bingjie Wang, Baohong Tian, Kexing Song, Zhe Chai* and *Yong Liu*

Hot deformation behavior of Cu–Ni–Si and Cu–Ni–Si–Ag alloys is investigated using the Gleeble-1500D simulator in the 600–800 °C deformation temperature and 0.01–5 s^{-1} strain rate ranges. Dynamic recrystallization (DRX) mechanism is a feature of high temperature flow stress–strain curves of the alloy. Microstructure is observed by optical microscopy. Ag addition can refine the grains and accelerate dynamic recrystallization. Characteristic points of the flow stress curves, including critical strain for DRX initiation (ε_c), are determined by employing strain hardening rate analysis. Processing maps are developed and analyzed based on the dynamic material model (DMM). Ag addition can optimize the alloy processing workability.

1. Introduction

Cu–Ni–Si is a multi-component copper alloy with high strength and electrical conductivity.[1,2] It also has high specific strength and outstanding electrical properties, along with excellent thermal conductivity. Therefore, Cu–Ni–Si alloys have many applications in aerospace and electronics industries as integrated circuit lead frame materials.[3,4] There are many materials research results related to Cu–Ni–Si alloys. Wang et al.[5] studied the Cu–7.4Ni–1.3Si–1.2Cr alloy and found that the thermal conductivity and tensile strength was 110 W mK^{-1} and 820 MPa, respectively. Liu et al.[6] calculated thermal activation energy $Q = 256.9$ kJ mol^{-1} for the Cu–2.0Ni–0.5Si–0.4Cr alloy. Huang et al.[7] developed the Cu–Ni–Si–Zn alloy, and identified the δ–Ni_2Si precipitating phase, which was responsible for the high hardness. Watanabe et al.[8] researched the effects of Ag addition on the Cu–Cr and Cu–Cr–Zr alloys. Small amounts of Ag can enhance strength, stress relaxation, and bending formability. Watanabe et al.[9] added 0.04 wt% of Ti to the Cu–Ni–Si alloy, which enhanced strength without affecting electrical properties. Previous research reports paid more attention to the Cu–Ni–Si alloy heat treatment process. During hot deformation, two kinds of softening behavior occur: dynamic recovery (DRV) and dynamic recrystallization (DRX). DRX can refine grains and improve plastic properties of materials, and also eliminate dislocations and cracks forming, during work hardening.[10] While material performance can be controlled by DRX, little attention has been paid to studying critical conditions of the Cu–Ni–Si alloy DRX behavior.

In this paper, experimental investigation of the Cu–Ni–Si–Ag alloy hot deformation behavior under different deformation conditions was carried out through single hot compression tests using the Gleeble-1500D simulator. The effects of different deformation conditions on the DRX behavior of the Cu–Ni–Si–Ag alloy are described in detail. In addition, the critical condition of DRX and processing maps with the strain of 0.1, 0.3, 0.4, and 0.5 are obtained. These results are helpful in optimizing the actual hot working process of the Cu–Ni–Si–Ag alloy to obtain suitable microstructure.

2. Experimental Section

The materials used in the present work were Cu–Ni–Si and Cu–Ni–Si–Ag alloys with the chemical composition in wt% Cu–2.0Ni–0.5Si and Cu–2.0Ni–0.5Si–0.15Ag, respectively. The

[*] *Dr. Y. Zhang, Dr. H. Sun, Dr. B. Wang, Dr. B. Tian, Dr. K. Song, Dr. Z. Chai, Dr. Y. Liu*
School of Materials Science and Engineering, Henan University of Science and Technology, Luoyang 471003, China
E-mail: zhshgu436@163.com
Dr. H. Sun, Dr. Y. Zhang, Dr. B. Wang, Dr. B. Tian, Dr. K. Song, Dr. Z. Chai, Dr. Y. Liu
Collaborative Innovation Center of Nonferrous Metals, Henan Province, Luoyang 471003, China
Dr. A. A. Volinsky, Dr. Y. Zhang
Department of Mechanical Engineering, University of South Florida, Tampa 33620, USA
E-mail: volinsky@usf.edu

[**] *This work was supported by the National Natural Science Foundation of China (51101052) and the National Science Foundation (IRES 1358088).*

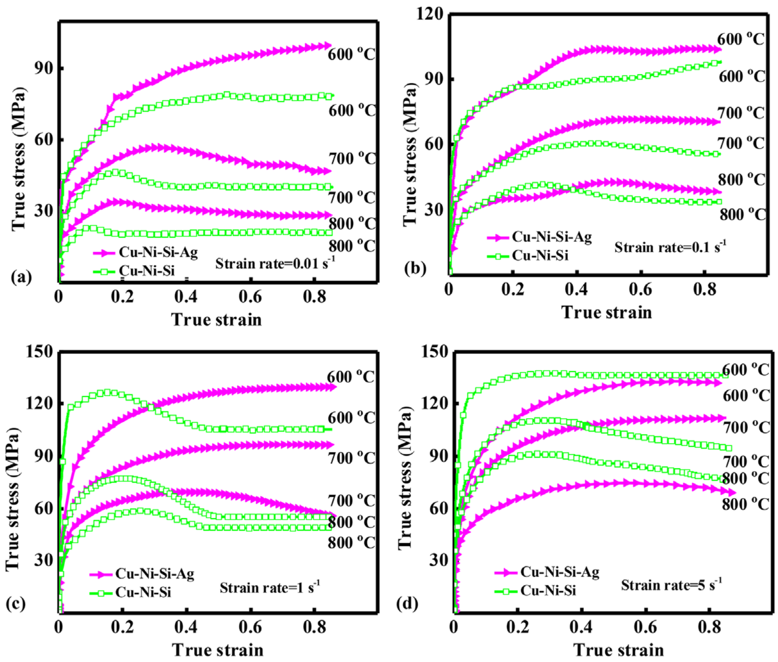

Fig. 1. True stress–strain curves of the Cu–Ni–Si and Cu–Ni–Si–Ag alloys under different deformation conditions.

alloys were smelted in a vacuum furnace in argon at 1200–1250 °C. Before the experiments, the ingots were homogenized at 850 °C for 2 h and cooled in water. They were machined into cylindrical specimens with 9 mm diameter and 15 mm length.

Hot compression tests were carried out using the Gleeble-1500D thermo-mechanical simulator, with the deformation temperature of 600–800 °C at 0.01–5 s^{-1} strain rate. The total deformation was about 60%. The specimens were heated to the deformation temperature at 10 °C s^{-1} heating rate, and then held for 5 min before compression. As soon as the compression tests were completed, the specimens were immediately water cooled to retain deformation microstructure, which was examined using Olympus PMG3 optical microscope. For optical microscopy, the specimens were mechanically polished and etched with $HCl + C_2H_5OH + FeCl_3$ solution.

3. Results and Discussion

3.1. Flow Stress Behavior

True stress–strain curves of the Cu–Ni–Si–Ag[10] and Cu–Ni–Si alloys under different hot deformation conditions are shown in Figure 1. The effects of deformation temperature and the initial strain rate on the flow stress are clear. The flow stress increases with the strain rate and decreases with deformation temperature. It is well known that hot deformation consists of two competing processes of strain work hardening and dynamic softening.[11]

It is clear that the flow stress for the Cu–Ni–Si–Ag alloy is higher than the Cu–Ni–Si alloy. At 0.3 true strain, 0.01 s^{-1} strain rate and 700 °C deformation temperature, the corresponding flow stresses are 47.89 and 56.61 MPa. The reason is because dislocation motion is restricted due to the Ag addition.

In this study, there are two softening mechanisms in the hot deformation process of the two alloys, namely dynamic recovery and dynamic recrystallization. True stress–strain curves with dynamic recovery characteristics are shown in Figure 1. The flow stress in the initial stage of deformation rapidly increases due to the work hardening. As strain continued to increase, a balance between the work hardening and dynamic recovery is reached, so the critical stress appeared to be constant. It can be seen that dynamic recovery was observed at the deformation temperatures of 600 °C in Figure 1a. Similar results were obtained at 700 °C deformation temperature in Figure 1b. True stress–strain curves with dynamic recrystallization characteristics are also presented in Figure 1. The flow stress increases to a peak value rapidly, and then begins to decrease until it reaches a relatively steady value and stays constant. This can be seen at 700 and 800 °C deformation temperatures in Figure 1a.

The true stress–strain curve at 600 °C deformation temperature in Figure 1a showed typical continuous strain hardening. The main reason for this is that the effect of work hardening is stronger than dynamic softening. Dislocations have more energy because of the rising temperature, and the dislocation density is increased because of external stress. When the dislocation density reaches a certain value, it can produce barriers, such as fixed dislocation tangles. The reason for the increasing stress is associated with increasing dislocation density. The strong interaction force between dislocations can effectively hinder dislocation movement.

3.2. Ag Effects on Deformation Activation Energy and Microstructure

The relationship between the strain rate, temperature, and the flow stress can be described by the Arrhenius equation[12]:

$$\dot{\varepsilon} = A[\sinh(\alpha\sigma)]^n \cdot \exp\left(-\frac{Q}{RT}\right) \tag{1}$$

Here, $\dot{\varepsilon}$ is the strain rate (s^{-1}), σ is the peak stress (MPa), Q is the activation energy of deformation (kJ mol^{-1}), R is the universal gas constant (8.314 kJ mol^{-1} K^{-1}), T is the temperature (K), A, n, and α are the materials constants.

Zhang et al.[13] calculated the materials constants n, β, α as 7.595, 0.137, 0.018, respectively, by using the cubic spline interpolation method. With the hyperbolic sine function, hot deformation activation energy $Q = 312.3$ kJ mol^{-1} and $A = 8.67 \times 10^{11}$. Constitutive equation for the Cu–Ni–Si–Ag alloy can be expressed as:

$$\dot{\varepsilon} = 8.67 \times 10^{11}[\sinh(0.018\sigma)]^{6.326} \exp\left(-\frac{312.3 \times 10^3}{RT}\right) \tag{2}$$

  ADVANCED ENGINEERING MATERIALS 2017, DOI: 10.1002/adem.201600607

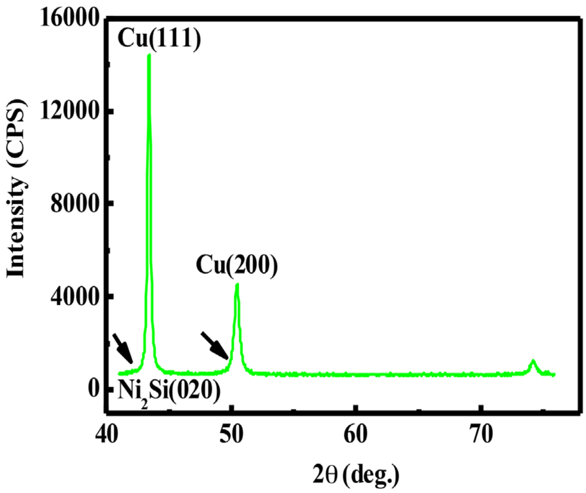

Fig. 2. XRD pattern of the Cu–Ni–Si–Ag alloy.

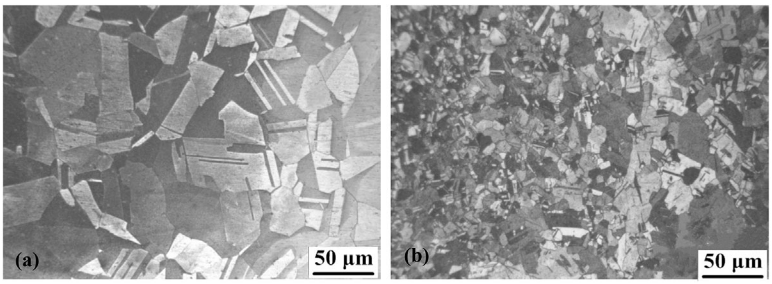

Fig. 3. Microstructure of (a) Cu–Ni–Si and (b) Cu–Ni–Si–Ag alloys after solution treatment at 900 °C for 1 h.

Zhang et al.[14] calculated hot deformation activation energy for the Cu–2.0Ni–0.5Si alloy as 245.4 kJ mol^{-1}, which is lower than for the Cu–2.0Ni–0.5Si–0.15Ag alloy. This is probably because the addition of small amounts of silver may inhibit dislocation motion. Figure 2 shows the X-ray diffraction pattern of the Cu–2.0Ni–0.5Si–0.15Ag alloy. Based on the XRD pattern, it is evident that the precipitation phase is Ni_2Si with $2\theta = 42.6°$. Ag addition can promote the Ni_2Si phase precipitation, which makes dislocations motion more difficult.

The microstructure of the Cu–Ni–Si and Cu–Ni–Si–Ag alloys after solution treatment is shown in Figure 3a and b. The grain size of the Cu–Ni–Si–Ag alloy is obviously smaller than the Cu–Ni–Si alloy. The average grain size of the Cu–Ni–Si alloy is 27.6 μm, while for the Cu–Ni–Si–Ag alloy, it is 22.4 μm. Therefore, one can safely draw the conclusion that the addition of Ag can refine the grain.

Figure 4 shows microstructure of the Cu–Ni–Si and Cu–Ni–Si–Ag alloys deformed at different strain rates and temperatures. Comparing Figure 4a and b, it can be seen that only elongated grains are found in Figure 4a, while the microstructure in Figure 4b has mixed elongated and small dynamic recrystallized grains. This means that the addition of Ag can refine the grain and effectively improve dynamic recrystallization. That is, because grain boundary sliding is the major deformation mechanism.[15–17] The alloy with Ag has smaller grains with more grain boundaries. New phase nucleation rate is higher, which is conducive to dynamic recrystallization. As observed, alloys recrystallization occurs, and the grain size of Cu–Ni–Si is 29 μm in Figure 4c, which is larger than 22.9 μm for the Cu–Ni–Si–Ag alloy in Figure 4d. This indicates that the Ag addition inhibits the DRX grains growth during hot deformation. Zhang et al.[2] also reported the same results in the study of the Cu–Cr–Zr–Ag alloy.

3.3. Critical Conditions for DRX of the Cu–Ni–Si–Ag Alloy

Dynamic recrystallization critical strain refers to the corresponding strain, at which dynamic recrystallization occurs during hot deformation. It is a key criterion for metal dynamic recrystallization to occur[18] and plays a pivotal role in studying metal hot deformation behavior. It is generally considered that DRX begins at the peak stress of the flow stress–strain curve.[19,20] However, this method is not applicable for the stress strain curves without apparent peak stress value. Poliak and Jonas[21] studied DRX of the AISI 321 steel and proved that the inflection in the work hardening rate-stress (θ-σ) plots is a better indication of DRX than the peak stress. Work hardening rate is the change of the flow stress with strain, which can effectively reflect changes in material internal structure. In many research reports,[22,23] work hardening rate was widely used to study dynamic recrystallization in steel, titanium,

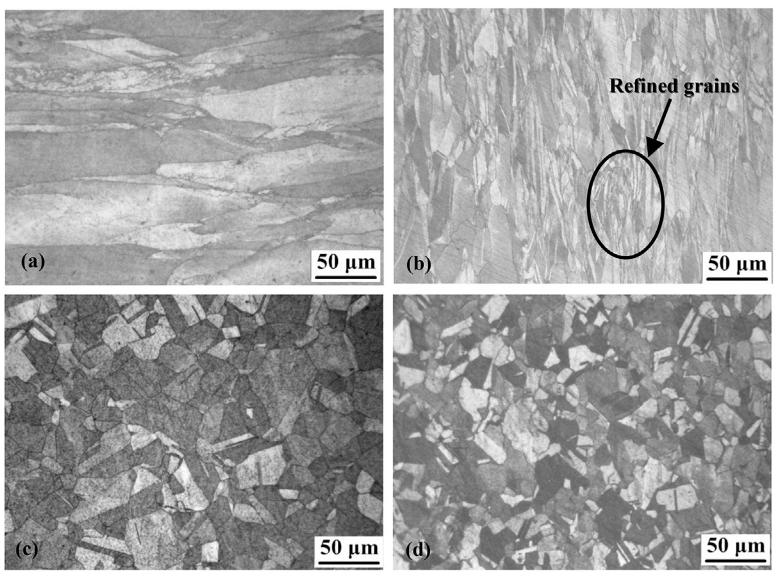

Fig. 4. Microstructure of (a) (c) Cu–Ni–Si and (b) (d) Cu–Ni–Si–Ag alloys; (a) 600 °C and 0.01 s^{-1}; (b) 600 °C and 0.01 s^{-1}; (c) 800 °C and 1 s^{-1}; and (d) 800 °C and 1 s^{-1}.

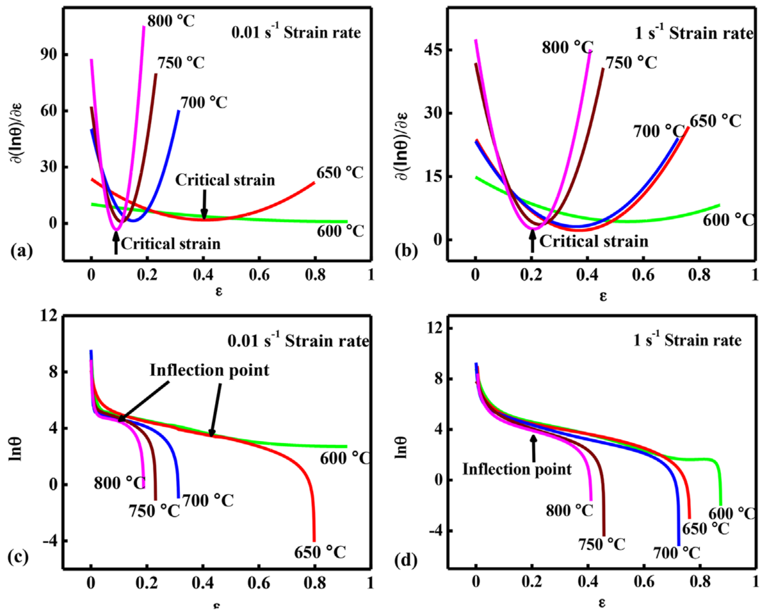

Fig. 5. (b) (d) Relationship between lnθ and ε; (a) (c) d(lnθ)/dε-ε versus ε plots for the Cu–Ni–Si–Ag alloy at different temperatures under the strain rate of 0.01 s^{-1} and 1 s^{-1}.

magnesium, and aluminum alloys, and showed high accuracy. Najafizadeh and Jonas obtained the critical stress to peak stress ratio of 0.875 for the 304H stainless steel, during hot deformation.[24]

The work hardening rate θ is the derivative of stress with respect to strain past the yield point. The strain hardening rate variations of the Cu–Ni–Si–Ag alloy under different deformation temperature and strain rate of 0.01 and 1 s^{-1} are shown in Figure 5b and d. Present research results show that, if the work hardening rate $\theta = 0$, work hardening and dynamic softening are in balance. After that, if the work hardening rate remains close to zero, dynamic recovery and work hardening are in balance and the stress–strain curves show characteristics of dynamic recovery. If the work hardening rate is greater than zero and constant, it indicates that the work hardening plays a leading role in hot working. If the work hardening rate drops to a negative value and, then, rises to a constant value, it shows that dynamic recrystallization occurred. According to Figure 5b and d, dynamic recrystallization occurred at 700, 750, and 800 °C with the 0.01 s^{-1} strain rate, and at 750 and 800 °C with the 1 s^{-1} strain rate.

In Figure 5a and c, dynamic recrystallization begins at the minimum value on the $-(d\theta/d\sigma)$ versus ε curve. It can be seen that all the curves have clear inflection points in Figure 5a and c and the critical stress in Figure 5b and d. According to Figure 5, the occurrence of DRX is much easier at high deformation temperature. The reason is because DRX is a thermally activated process. At higher temperature, the Cu–Ni–Si–Ag alloy can accumulate enough energy for nucleation and growth of the DRX grains.

3.4. Processing Maps and Microstructure Evolution of the Cu–Ni–Si–Ag Alloy

The processing map is a combination by superimposition of power dissipation and instability maps. It is an effective tool to design and optimize the hot working process. Many researchers show that the instantaneously dissipated power consists of the two complementary parts. One is related to power dissipation through plastic deformation, most of which is converted into plastic heat and the other represents power dissipation by microstructure transition, such as phase transformations, dynamic recrystallization, as well as wedge cracking.

Processing maps can be constructed by using the principles of the dynamic materials model (DMM).[25,26] Prasad and Seshacharyulu[27] reported

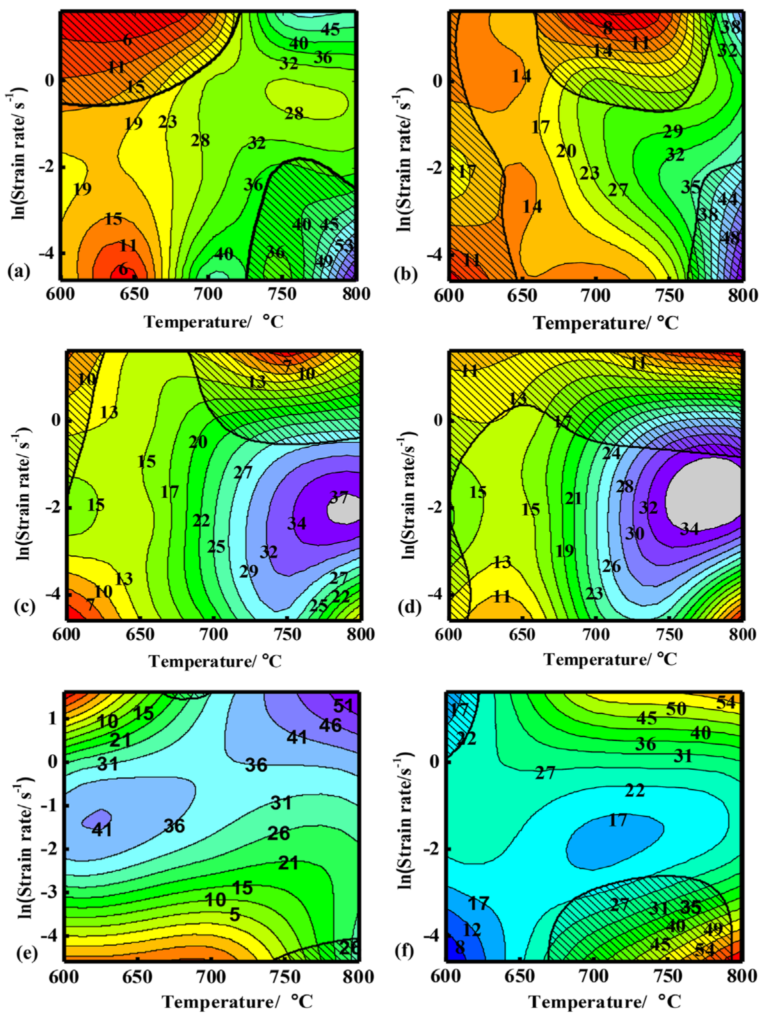

Fig. 6. Processing maps of (e, f) the Cu–Ni–Si and (a–d) Cu–Ni–Si–Ag alloys at different strains (a) ε = 0.1; (b) ε = 0.3; (c) ε = 0.5; (d) ε = 0.6; (e) ε = 0.1; and (f) ε = 0.3.

DOI: 10.1002/adem.201600607

that the relationship between the flow stress and the strain rate in the hot deforming part at a given temperature and strain can be expressed as:

$$\sigma = K\dot{\varepsilon}^{m} \tag{3}$$

Here, K is a constant and m is the strain rate sensitivity exponent defined as:

$$m = \frac{\dot{\varepsilon}\, d\,\sigma}{\sigma\, d\,\dot{\varepsilon}} = \left[\frac{\partial(\ln\sigma)}{\partial(\ln\dot{\varepsilon})}\right]_{\varepsilon,T} \cong \frac{d\ln\sigma}{d\ln\dot{\varepsilon}} \tag{4}$$

The efficiency of power dissipation, η, as the measure of material's workability, was determined using the formula proposed by Prasad and Seshacharyulu for the DMM model:

$$\eta = \frac{J}{J_{\max}} = \frac{2m}{m+1} \times 100\% \tag{5}$$

Based on the irreversible thermodynamics extremum principle, the instability map can be applied as a continuous instability criterion by using dimensionless factor $\xi(\dot{\varepsilon})$ to describe large plastic deformation. Prasad and Seshacharyulu[28] had deduced the instability criterion expression for materials by using the following maximum entropy principle:

$$\xi(\dot{\varepsilon}) = \frac{\partial \ln[m/(m+1)]}{\partial \ln \dot{\varepsilon}} + m < 0 \tag{6}$$

Figure 6 shows the processing maps of the Cu–Ni–Si and Cu–Ni–Si–Ag alloys at true strains of 0.1, 0.3, 0.5, and 0.6. It can be seen that there are two domains in the processing maps, one is the instability domain, which was painted with the shadow, and another is the stabile domain. The contour numbers represent the efficiency of power dissipation in percent, which indicates the microstructure changes during hot deformation. Higher values are beneficial for plastic forming.

As seen in Figure 6, the distribution characteristics of the energy dissipation are similar, which increases with temperature and strain rate. It can be seen that the instability regions were significantly affected by the strain, and the instability region area increases with the strain, as demonstrated by other researchers.[29–31] Materials deformed in high efficiency power dissipation region have good workability. Thus, the deformation temperature and strain rate have the high value of η in the stability domain of the processing map, which can be considered optimal hot working parameters. Figure 6d shows the processing map of the Cu–Ni–Si–Ag alloy with the 0.6 strain, where maps can be divided into three typical domains. The first domain is at the higher strain rate, with the efficiency increase from 11 to 34%. Typical microstructure of this alloy deformed in this domain at 650 °C and 1 s^{-1} is shown in Figure 7b. The average grain size is 32.2 μm with mixed-grain microstructure.[32] There are many elongated grains and some recrystallization grains can be observed around the grain boundaries. Localized shear is caused by high strain rates, which leads to inconsistent mechanical properties. The second domain is at the low strain rate and low deformation temperature. Figure 7a shows the alloy microstructure deformed at 650 °C and 0.01 s^{-1} strain rate. It presents many elongated grains with the average grain size of 15.7 μm and more dynamic recrystallization grains. There are parallels between the two above cases. The necklace structures around the elongated grain boundaries are found in the two images. This means that the main softening mechanism is dynamic recovery in this domain. Many research results indicate that the alloy easily fractures during deformation processing at this condition.[33] The above areas of unstable domains should be avoided in hot working. The last domain shows the alloy, which is deformed in the higher temperature range of 700–800 °C, and lower strain rate range of 0.01–0.33 s^{-1}. Optical images of the Cu–Ni–Si–Ag alloy microstructure deformed at 750 and 800 °C, with the same strain rate of 0.01 s^{-1} are shown in Figure 7c and e. The original defective grains have been almost completely replaced by the recrystallized grains. The formation of a large number of equiaxial grains indicates that the DRX process is almost complete. Comparing the grain size in

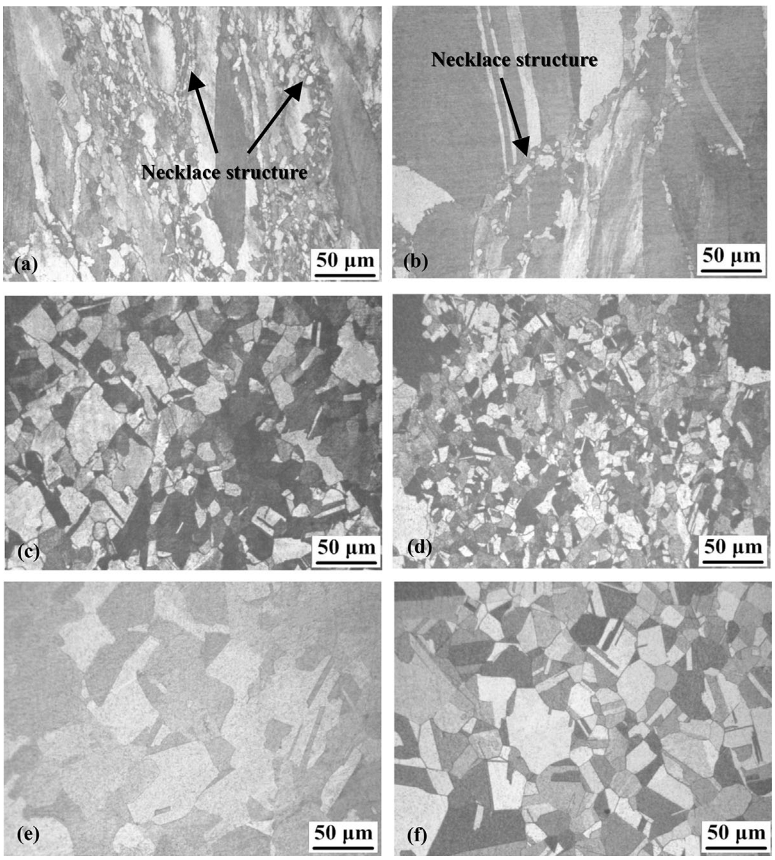

Fig. 7. Optical micrographs of the Cu–Ni–Si–Ag alloy deformed at (a) 650 °C and 0.01 s^{-1}; (b) 650 °C, 1 s^{-1}; (c) 750 °C; 0.01 s^{-1}; (d) 750 °C, 0.1 s^{-1}; (e) 800 °C, 0.01 s^{-1}; and (f) 800 °C, 0.1 s^{-1}.

DOI: 10.1002/adem.201600607

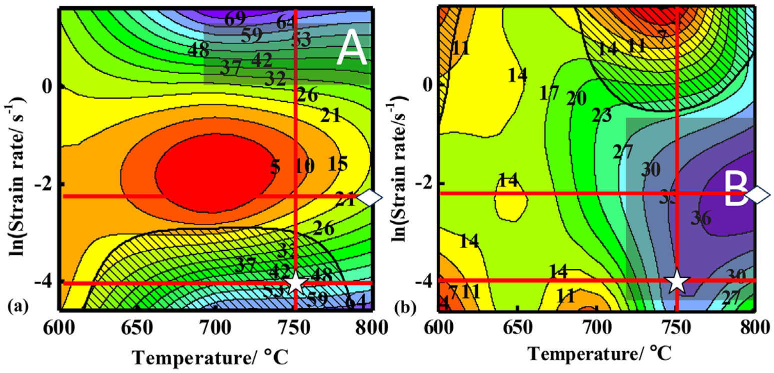

Fig. 8. Processing maps of (a) Cu–Ni–Si and (b) Cu–Ni–Si–Ag alloys at 0.4 strain.

Figure 7c and e, the average size of these grains in Figure 7d is 15.8 μm. It is coarser than the 31 μm average grain size in Figure 7c. The average grain size in Figure 7e and f is 83.6 and 34 μm, respectively. Figure 7c shows the average grain size of 15.2 μm, which is larger than in Figure 7d. The grain size in Figure 7e is also larger than in Figure 7f. Higher temperature and lower strain rate can promote dynamic recrystallization and increase the grain size. Moreover, the peak efficiency in this domain is 34%, which is consistent with the research of Zhang et al.[26] As a result, the optimal processing parameters of hot working for the Cu–Ni–Si–Ag alloy are at 700–800 °C and 0.01–0.46 s^{-1}, and the efficiency of power dissipation is 23–34%.

Comparing Figure 6a and e with b and f, the contour lines of Cu–Ni–Si are sparser than the Cu–Ni–Si–Ag alloy. Under high temperature and low strain rate region, which has higher power dissipation, the stability region for the Cu–Ni–Si–Ag alloy is much wider than for the Cu–Ni–Si alloy. This means that with the same processing conditions, the workability of the Cu–Ni–Si–Ag alloy is better than the Cu–Ni–Si alloy.

4. Discussion

Figure 8a and b show the processing maps of the Cu–Ni–Si and Cu–Ni–Si–Ag alloys at 0.4 strain. It shows that the area of the optimal processing parameters of Cu–Ni–Si (region A) is smaller than Cu–Ni–Si–Ag (region B). Efficiency of energy dissipation (η) in Figure 8a fluctuates strongly, while the value of Cu–Ni–Si–Ag is stable. This means that Ag addition can improve hot workability of the Cu–Ni–Si alloy.

Microstructure of the Cu–Ni–Si and Cu–Ni–Si–Ag alloys deformed at various conditions is shown in Figure 9. Microstructure of the two alloys deformed at 750 °C and 0.01 s^{-1} (marked by the star in Figure 8) is shown in Figure 9a and b. It is clear that smaller and elongated grain structures exist in the Cu–Ni–Si alloy. In actual manufacturing practice, these areas are unstable and unsafe, and should be avoided. At the same conditions, smaller grains are found in the microstructure of the Cu–Ni–Si–Ag alloy, where DRX has occurred. The efficiency of the Cu–Ni–Si–Ag alloy is 32% in Figure 8b. Comparing Figure 9c and d, uniform and equiaxial grains are observed in the Cu–Ni–Si–Ag alloy. Some twins are observed in Figure 9c. DRX has also occurred, but was incomplete. Coarser DRX grains can be observed in the microstructure. This also means that the domain at this hot deformation condition is unstable. This indicates that the addition of Ag can refine the grains and improve DRX. The reason is that the grain boundaries increase gradually with the addition of Ag, and the DRX nucleation is improved.[34]

Figure 10 shows the plots of $d(\ln\theta)/d\varepsilon$-$\varepsilon$ versus ε for the Cu–Ni–Si–Ag and Cu–Ni–Si alloys under different strain rates at 700 °C. It is quite clear that the critical strain point for DRX of the Cu–Ni–Si is lower than the Cu–Ni–Si–Ag alloy under the same deformation conditions. The reason is that the addition of Ag is beneficial for the precipitated phase. Precipitated phase formation is favorable for the subgrain stability, which hinders dislocation motion and slows down dynamic recrystallization, during hot deformation. In the initial process, the addition of Ag can improve the phases rapidly precipitated from the matrix, and more precipitated phases can be obtained in the Cu–Ni–Si–Ag alloy than in the Cu–Ni–Si alloy. Thus, at the initial hot deformation stage, the DRX of the Cu–Ni–Si alloy will occur at lower strain. Only when the strain is high enough, DRX of the Cu–Ni–Si–Ag alloy can occur. As hot deformation progresses, the amount of precipitated phases no longer increases. Grain refinement effect becomes more evident

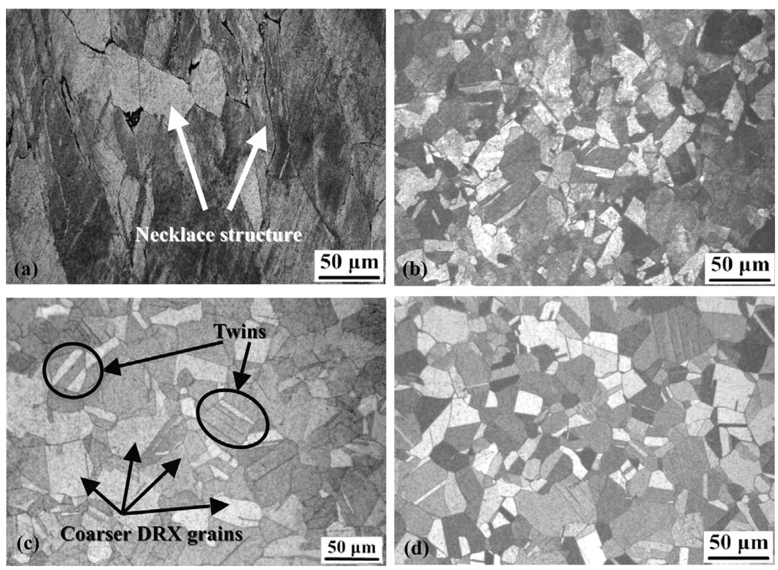

Fig. 9. Microstructure of (a) (c) Cu–Ni–Si and (b) (d) Cu–Ni–Si–Ag alloys; (a) 750 °C and 0.01 s^{-1}; (b) 750 °C and 0.01 s^{-1}; (c) 800 °C and 0.1 s^{-1}; and (d) 800 °C and 0.1 s^{-1}.

ADVANCED ENGINEERING MATERIALS 2017, DOI: 10.1002/adem.201600607

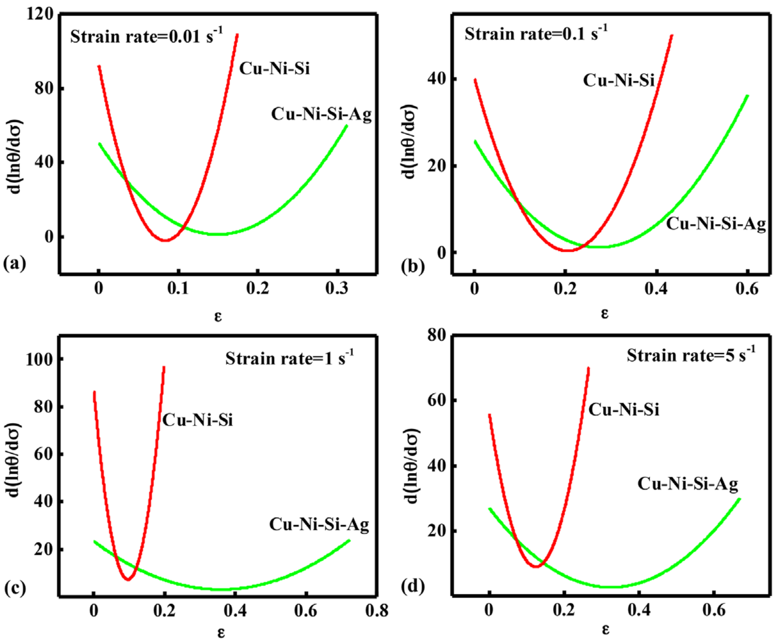

Fig. 10. d(lnθ)/dε-ε versus ε plots for the Cu–Ni–Si–Ag and Cu–Ni–Si alloys under the strain rate of 0.01 s^{-1}, 0.1 s^{-1}, 1 s^{-1}, and 5 s^{-1} at 700 °C.

with the addition of Ag, and DRX occurs. Zhang et al.[35] also reported the same results in the study of the Cu–Ni–Si–Ag alloy.

5. Conclusions

Hot compression tests of Cu–Ni–Si and Cu–Ni–Si–Ag alloys were performed at different deformation conditions. The stress–strain data were carefully analyzed. The DRX behavior and hot workability of the alloy have been systematically investigated. Based on the results, the following conclusions can be drawn:

1) Dynamic recrystallization mechanism is the main softening mechanism for the Cu–Ni–Si and Cu–Ni–Si–Ag alloys, during hot deformation. The stress increases with decreasing deformation temperature or increasing strain rate.
2) The dynamic recrystallization critical strain is closely related to temperature and strain rate. Higher deformation temperature or lower strain rate can promote dynamic recrystallization.
3) The optimal processing parameters for the Cu–Ni–Si–Ag alloy were obtained through the processing maps: 700–800 °C and 0.01–0.46 s^{-1} strain rate. The efficiency of power dissipation is 23–34%, during the hot deformation process. The addition of Ag can effectively optimize the workability of the Cu–Ni–Si alloy.
4) Dynamic recrystallization occurs at high temperature and low strain rate. The microstructure is strongly affected by the deformation temperature and the strain rate. Ag addition can refine the grains and advance dynamic recrystallization effectively.

Article first published online: xxxx
Manuscript Revised: December 24, 2016
Manuscript Received: August 29, 2016

[1] D. P. Lu, J. Wang, W. J. Zeng, Y. Liu, L. Lu, B. D. Sun, *Mater. Sci. Eng. A* **2016**, *421*, 254.
[2] Y. Zhang, B. H. Tian, A. A. Volinsky, X. H. Chen, H. L. Sun, Z. Chai, P. Liu, Y. Liu, *J. Mater. Res*. **2016**, *31*, 1275.
[3] M. Gotoa, S. Z. Han, S. H. Lim, J. Kitamura, T. Fujimura, J. H. Ahn, T. Yamamoto, S. Kim, J. Lee, *Int. J. Fatigue* **2016**, *87*, 15.
[4] A. Khereddine, F. H. Larbi, L. Djebala, H. Azzeddine, B. Alili, D. Bradai, *Trans. Nonferrous Met. Soc. China* **2011**, *21*, 482.
[5] H. S. Wang, H. G. Chen, J. W. Gu, C. E. Hsu, C. Y. Wu, *Mater. Sci. Eng. A* **2014**, *619*, 221.
[6] P. Liu, Y. Zhang, L. Fan, B. H. Tian. *Rare Met. Mater. Eng*. **2009**, *38*, 33.
[7] F. X. Huang, J. S. Ma, H. L. Ning, Y. W. Cao, Z. T. Geng. *Mater. Lett*. **2003**, *57*, 2135.
[8] C. Watanabe, M. Ryoichi, T. Kazue. *J. Mater. Sci*. **2008**, *43*, 813.
[9] C. Watanabe, S. Takeshita, R. Monzen, *Metall. Mater. Trans. A* **2015**, *46*, 2469.
[10] Y. Zhang, P. Liu, B. H. Tian, S. Zhang, X. H. Chen, S. G. Jia, Y. Liu, *J. Funct. Mater*. **2010**, *30*, 787.
[11] J. R. Cao, Z. D. Liu, S. C. Cheng, G. Yang, J. X. Xie, *Acta Metall. Sin*. **2007**, *43*, 35.
[12] S. Arrhenius, *Z. Phys. Chem*. **1889**, *4*, 226.
[13] Y. Zhang, P. Liu, B. H. Tian, X. H. Chen, S. G. Jia, *T. Mater. Heat Treat*. **2008**, *29*, 71.
[14] Y. Zhang, P. Liu, B. H. Tian, S. G. Jia, L. Fan. *J. Funct. Mater*. **2010**, *41*, 446.
[15] M. Bacca, R. M. McMeeking, *Int. J. Plast*. **2016**, *83*, 74.
[16] T. G. Langdon, *Acta Metall. Mater*. **1994**, *42*, 2437.
[17] A. Chokshi, A. Rosen, J. Karch, H. Gleiter, *Scr. Metall*. **1989**, *23*, 1679.
[18] H. Mirzadeh, A. Najafizadeh, *Mater. Des*. **2010**, *31*, 1174.
[19] E. I. Poliak, J. J. Jonos, *Acta Mater*. **1996**, *44*, 127.
[20] J. T. Liu, G. Q. Liu, B. F. Hu, Y. P. Song, Y. W. Zhang, *Trans. Mater. Heat. Treat*. **2004**, *25*, 25.
[21] E. I. Poliak, J. J. Jonos, *ISIJ Int*. **2003**, *43*, 692.
[22] E. S. Puchi-Cabrera, M. H. Staia, J. D. Guerin, J. Lesage, M. Dubar, D. Chicot, *Int. J. Plast*. **2013**, *51*, 145.
[23] Y. J. Zhao, A. L. Hu, Y. T. Li, X. Z. Pang, *Trans. Mater. Heat. Treat*. **2012**, *37*, 20.
[24] A. Najafizadeh, J. J. Jonas, *ISIJ Int*. **2006**, *46*, 1679.
[25] Z. Y. Ding, S. G. Jia, P. F. Zhao, M. Deng, K. X. Song, *Mater. Sci. Eng. A* **2013**, *570*, 87.
[26] Y. Zhang, P. Liu, B. H. Tian, Y. Liu, R. Q. Li, Q. Q. Xu, *Trans. Nonferrous Met. Soc. China* **2013**, *23*, 2341.
[27] Y. V. R. K. Prasad, T. Seshacharyulu, *Mater. Sci. Eng. A* **1998**, *243*, 82.

[28] Y. V. R. K. Prasad, T. Seshacharyulu, *Int. Mater. Rev.* **1998**, *43*, 243.

[29] Y. Wang, Q. L. Pan, Y. F. Song, C. Li, Z. F. Li, *Mater. Des.* **2013**, *51*, 154.

[30] J. C. Luo, L. Li, M. Q. Li, *Mater. Sci. Eng. A* **2014**, *606*, 165.

[31] Y. Zhang, Z. Chai, A. A. Volinsky, B. H. Tian, H. L. Sun, P. Liu, Y. Liu, *Mater. Sci. Eng. A* **2016**, *662*, 320.

[32] S. Wang, L. G. Hou, J. R. Luo, J. S. Zhang, L. Z. Zhuang, *J. Mater. Process. Tech.* **2015**, *225*, 110.

[33] T. Xi, C. G. Yang, M. B. Shahzad, K. Yang, *Mater. Des.* **2015**, *87*, 303.

[34] Y. Y. Chen, B. H. Li, F. T. Kong, *Trans. Nonferrous Met. Soc.* **2007**, *17*, 58.

[35] P. Liu, Y. Zhang, B. H. Tian, X. H. Chen, S. G. Jia, F. Z. Ren, Y. Q. Long, *J. Funct. Mater.* **2008**, *39*, 257.

ADVANCED ENGINEERING MATERIALS **2017**,
DOI: 10.1002/adem.201600607